TOA Lightning Location Retrieval on Spherical and Oblate Spheroidal Earth Geometries

W. J. KOSHAK

Global Hydrology and Climate Center, NASA Marshall Space Flight Center, Huntsville, Alabama

R. J. SOLAKIEWICZ

Department of Mathematics and Computer Science, Chicago State University, Chicago, Illinois

(Manuscript received 7 December 1999, in final form 19 April 2000)

ABSTRACT

A simple linear algebraic solution is introduced for retrieving the location and time-of-occurrence of lightning ground strikes on a spherical earth from a network of four or more time-of-arrival sensors. Since the solution accounts for earth curvature, it represents an extension to earlier planar model results. A test of the retrieval method is provided using computer-simulated datasets. The method is easy to comprehend and completely avoids reference to the mathematics of spherical hyperbolas. An extension to the spherical earth solution is provided for an oblate spheroidal earth geometry, and the importance/relevance of oblate effects are discussed. Future application of these methods in support of the North American National Lightning Detection Network is desirable, but additional theoretical investigations are required to incorporate magnetic bearing information into the present solution process.

1. Introduction

Recently, Koshak et al. (2000) introduced a linear planar (LP) method for determining the location and time-of-occurrence of cloud-to-ground lightning using a network of Advanced Lightning Direction Finder (ALDF) sensors. The study demonstrated how radio frequency arrival time, bearing, and signal amplitude ALDF data could be *simultaneously* analyzed to determine the ground discharge location on a flat earth. Because solutions were obtained by inverting a single system of linear equations that included all the ALDF data and because the linear system could be easily modified if some ALDF data were not available, numerical coding of the LP method was particularly easy and the method itself highly flexible.

Based on computer-simulated tests, the LP method located lightning to within about 1 km, provided the discharges were within a few hundred kilometers of the (four station) ALDF network. Sources within the area bounded by the ALDF sensors could be located to within 200 m. By comparison, the nadir resolution of the National Aeronautics and Space Administration's (NASA's) space-based, low earth-orbiting lightning detectors, the Optical Transient Detector (OTD) and the Lightning Imaging Sensor (LIS), are 10 km and 4 km, respectively (Christian et al. 1992; Boccippio et al. 2000). Hence, it was concluded that the LP method is useful for validating the location accuracy of OTD and LIS (Koshak et al. 2000).

Assuming four or more sensors are available, the LP method can be used to determine lightning locations using just arrival time data. For the case of four arrival time measurements (t_1, t_2, t_3, t_4) from sensors located at $[(x_1, y_1), (x_2, y_2), (x_3, y_3), (x_4, y_4)]$, the LP method reduces to the linear system

$$\begin{bmatrix} g_1 \\ g_2 \\ g_3 \end{bmatrix} = \begin{bmatrix} (x_2 - x_1) & (y_2 - y_1) & c^2(t_1 - t_2) \\ (x_3 - x_1) & (y_3 - y_1) & c^2(t_1 - t_3) \\ (x_4 - x_1) & (y_4 - y_1) & c^2(t_1 - t_4) \end{bmatrix} \begin{bmatrix} x \\ y \\ t \end{bmatrix}, \quad (1)$$

where the elements of the column vector on the left-hand side are nonlinear functions of the arrival time measurements and the sensor locations. Again, the retrieval is fundamentally planar, since the retrieved source location is in terms of the Cartesian coordinates (x, y). The retrieved time-of-occurrence of the discharge is t. See Koshak et al. (2000) for additional details.

In the current work, the LP approach is extended to account for earth curvature. The new formulation is called a linear spherical (LS) method. Because spherical earth curvature effects are accounted for, the LS method

Corresponding author address: Dr. William J. Koshak, NASA–MSFC/SD60, Global Hydrology and Climate Center, 320 Sparkman Dr., Huntsville, AL 35805.
E-mail: william.koshak@msfc.nasa.gov

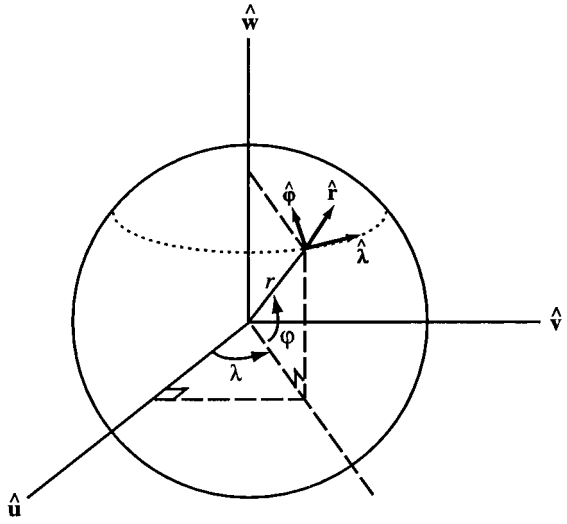

FIG. 1. Spherical coordinate system used for the LS method.

will retrieve distant lightning sources more accurately than the LP method, thereby increasing the area over which OTD/LIS data can be ground-validated. Like the LP approach, the LS method determines source location from four or more arrival time measurements, but instead of expressing the source solution in Cartesian coordinates (x, y), it is expressed in terms of latitude and longitude coordinates (φ, λ). Moreover, the simple LS method completely avoids reference to the mathematics of spherical hyperbolas such as those discussed in Lewis (1960, 1964).

In addition, a quasi-analytic extension to the LS method is provided to accommodate an oblate spheroidal earth geometry. The distance between a lightning source and a time-of-arrival (TOA) sensor is measured along a geodesic and can be expressed in terms of an elliptic integral. The importance/relevance of oblate effects are discussed using computer-simulated sources and simulated arrival time errors.

2. LS method for spherical earth

It is assumed that four or more ($n \geq 4$) TOA sensors are available for determining the latitude/longitude location of a cloud-to-ground lightning event on a spherical earth surface. To solve this problem, a spherical coordinate system, as shown in Fig. 1, is used. By definition, the prime meridian is associated with longitude $\lambda = 0$ and the equator with latitude $\varphi = 0$. The spherical earth radius is denoted by the variable r. If $\mathbf{r} = r\hat{\mathbf{r}}$ is the lightning source location and $\mathbf{r}_i = r\hat{\mathbf{r}}_i$ is the location of the ith sensor, the unit vectors can be written as (see Fig. 1)

$$\hat{\mathbf{r}}_i = \cos\varphi_i \cos\lambda_i \hat{\mathbf{u}} + \cos\varphi_i \sin\lambda_i \hat{\mathbf{v}} + \sin\varphi_i \hat{\mathbf{w}},$$

$$\hat{\mathbf{r}} = \cos\varphi \cos\lambda \hat{\mathbf{u}} + \cos\varphi \sin\lambda \hat{\mathbf{v}} + \sin\varphi \hat{\mathbf{w}}. \quad (2)$$

So the spherical form of the arrival time equation becomes

$$t_i = t + \frac{1}{c} r\theta_i, \quad (3)$$

where t is the time of occurrence of the lightning at $\mathbf{r}$, t_i is the arrival time measurement at $\mathbf{r}_i$, and θ_i is the angle between the unit vectors in (2) given by

$$\theta_i = \cos^{-1}(K_{i1} \cos\varphi \cos\lambda + K_{i2} \cos\varphi \sin\lambda + K_{i3} \sin\varphi), \quad (4)$$

with $K_{i1} = \cos\varphi_i \cos\lambda_i$, $K_{i2} = \cos\varphi_i \sin\lambda_i$, and $K_{i3} = \sin\varphi_i$. Note that the value $r\theta_i$ is the great circle distance between the lightning and the ith sensor. Using (4) and a standard trigonometric identity, (3) can be written as (for $i = 1, 2, \ldots, n$)

$$\cos\frac{c}{r}t_i \cos\frac{c}{r}t + \sin\frac{c}{r}t_i \sin\frac{c}{r}t = K_{i1} \cos\varphi \cos\lambda + K_{i2} \cos\varphi \sin\lambda + K_{i3} \sin\varphi. \quad (5)$$

At this point, several different approaches can be used to obtain a final solution. For example, we can divide (5) by $\sin(ct/r)$ to obtain the linear system

$$g_i = K_{i1} f_1 + K_{i2} f_2 + K_{i3} f_3 + K_{i4} f_4, \quad (6)$$

where $g_i = \sin(ct_i/r)$, $f_1 = \cos\varphi \cos\lambda/\sin(ct/r)$, $f_2 = \cos\varphi \sin\lambda/\sin(ct/r)$, $f_3 = \sin\varphi/\sin(ct/r)$, and $f_4 = \cot(ct/r)$. The additional coefficient is $K_{i4} = -\cos(ct_i/r)$. The equations in (6) can be written in matrix form as $\mathbf{g} = \mathbf{K}\mathbf{f}$, with direct solution $\mathbf{f} = \mathbf{K}^{-1}\mathbf{g}$ ($n = 4$) and least squares solution $\mathbf{f} = (\tilde{\mathbf{K}}\mathbf{K})^{-1}\tilde{\mathbf{K}}\mathbf{g}$ ($n > 4$). Here, the tilde indicates matrix transposition. The source location and time of occurrence can be extracted from $\mathbf{f}$ as follows:

$$\varphi = \tan^{-1}\left(\frac{f_3}{f_1}\cos\lambda\right), \qquad \lambda = \tan^{-1}\left(\frac{f_2}{f_1}\right),$$

$$t = \frac{r}{c}\cot^{-1} f_4. \quad (7)$$

Since $\mathbf{K} = \mathbf{K}(\varphi_i, \lambda_i, t_i)$, each element of $\mathbf{K}$ depends on where the TOA network is located on the surface of the earth and on what convention is used for timing lightning radio waves (e.g., UTC converted to seconds, GPS, TAI). Numerical variation in $\mathbf{K}$ implies variation in the eigenvalues of $\mathbf{K}$ and variation in the elements of $\mathbf{K}^{-1}$ or $(\tilde{\mathbf{K}}\,\mathbf{K})^{-1}$. This ultimately means that numerical magnification of the measurement errors in $\mathbf{g}$ depends on where the network is located (see Twomey 1977, chapter 6 for a detailed discussion of error magnification in inversion problems). Since in this writing we will want to characterize retrieval errors (see sections 3, 5, and 6 to follow), for experimental networks located anywhere in the world, it is beneficial to avoid using the solution scheme in (7) in favor of a more ''standardized matrix.'' That is, one whose matrix elements do not differ between, say, a hypothetical network in Italy (that

recorded times by converting a UTC format into seconds) compared to one in Japan (that recorded time in GPS seconds).

To obtain the standard matrix, we will *rotate* the spatial coordinates in the problem and *translate* the temporal coordinate.

Note that the form in (5) as well as θ_i are invariant under spatial coordinate system rotations. If one rotates the coordinate system ($\hat{\mathbf{u}}$, $\hat{\mathbf{v}}$, $\hat{\mathbf{w}}$) into ($\hat{\mathbf{u}}'$, $\hat{\mathbf{v}}'$, $\hat{\mathbf{w}}'$) by an (Euler) angle λ_1 about $\hat{\mathbf{w}}$, and then ($\hat{\mathbf{u}}'$, $\hat{\mathbf{v}}'$, $\hat{\mathbf{w}}'$) is rotated into ($\hat{\mathbf{u}}^*$, $\hat{\mathbf{v}}^*$, $\hat{\mathbf{w}}^*$) by an Euler angle φ_1 about $-\hat{\mathbf{v}}'$, (5) maintains the same form in the starred system

$$\cos\frac{c}{r}t_i \cos\frac{c}{r}t + \sin\frac{c}{r}t_i \sin\frac{c}{r}t = K_{i1}^* \cos\varphi^* \cos\lambda^* + K_{i2}^* \cos\varphi^* \sin\lambda^* + K_{i3}^* \sin\varphi^*. \quad (8)$$

Here, (K_{i1}^*, K_{i2}^*, K_{i3}^*) are identical to the expressions for (K_{i1}, K_{i2}, K_{i3}) but with (φ_i, λ_i) replaced by (φ_i^*, λ_i^*).

In (5), latitude and longitude are referenced to the equator and prime meridian, but in (8), all locations are expressed relative to site 1. This fact will help simplify the mathematics, since ($\varphi_1^* \equiv 0$, $\lambda_1^* \equiv 0$). If one now invokes the convention that site 1 excites at $t_1 = 0$, the transit equation in (8), evaluated at $i = 1$, is

$$\cos\frac{c}{r}t = \cos\varphi^* \cos\lambda^*. \quad (9)$$

Since $t_1 = 0$ and causality dictates that $t \le t_1$, then $t \le 0$ must hold. Hence, $\sin(ct/r) = -|\sin(ct/r)| = -(\sin^2 ct/r)^{1/2}$ or

$$\sin\frac{c}{r}t = -\left(1 - \cos^2\frac{c}{r}t\right)^{1/2} = -(1 - \cos^2\varphi^* \cos^2\lambda^*)^{1/2}. \quad (10)$$

Using (9) and (10) to eliminate time in favor of space, (8) becomes (for $i = 2, 3, \ldots, n$)

$$a_{i-1} = L_{i-1,1}h_1 + L_{i-1,2}h_2 + L_{i-1,3}h_3, \quad (11)$$

where $a_{i-1} = \sin(ct_i/r)$, $L_{i-1,1} = \cos\varphi_i^* \cos\lambda_i^* - \cos(ct_2/r)$, $L_{i-1,2} = \cos\varphi_i^* \sin\lambda_i^*$, $L_{i-1,3} = \sin\varphi_i^*$, $h_1 = \Psi^* \cos\varphi^* \cos\lambda^*$, $h_2 = \Psi^* \cos\varphi^* \sin\lambda^*$, $h_3 = \Psi^* \sin\varphi^*$, and $\Psi^* = -(1 - \cos^2\varphi^* \cos^2\lambda^*)^{-1/2}$. The linear system in (11) can be written in matrix/vector form as

$$\mathbf{a} = \mathbf{L}\mathbf{h}, \quad (12)$$

with direct and least squares solutions given respectively as

$$\mathbf{h} = \mathbf{L}^{-1}\mathbf{a} \quad (n = 4), \qquad \mathbf{h} = (\tilde{\mathbf{L}}\mathbf{L})^{-1}\tilde{\mathbf{L}}\mathbf{a} \quad (n > 4). \quad (13)$$

Unlike the variable $\mathbf{K}$ matrix, $\mathbf{L} = \mathbf{L}(\varphi_k^*, \lambda_k^*, t_k)$ does not depend on *where* the network is located on the earth (e.g., Italy or Japan). It depends only on the specific *network geometry*, that is, on the location of the sites *relative to site 1* and on the arrival times recorded at each site. In other words, if the hypothetical experimenters in Italy and Japan were to pick the same network geometry for their respective networks and if each network measured identically the same set of arrival times t_k, then the $\mathbf{L}$ matrix used by the Italian experimenters would be identical to the $\mathbf{L}$ matrix used by the Japanese. Hence, given the network geometry and a set of measurements t_k, (12) is a standardized linear system that produces the same lightning location retrieval error results *no matter where the network is located on the surface of the earth.*

Assuming that the Italian and Japanese networks have identical network geometries, we next clarify what conditions are sufficient in order that the set of times t_k from the Italian network are equivalent to the Japanese network. First, the two groups of experimenters should use the same units of time (e.g., seconds). Second, these times should be referenced to the excitation time of ''site 1'' (say the central site of each network). Third, the measurement timing errors produced from each network must be the same. Fourth, even if the above conditions are met, lightning location relative to each network is important. For example, a lightning source 100 km due east of the Italian network would produce a set of arrival times that would differ from a source 300 km due north of the Japanese network. However, if each source is 100 km due east of each network, the arrival times would be the same. If all four of these conditions are met, the $\mathbf{L}$ matrix for these two hypothetical networks would be identical, and *the spatial distribution of lightning location retrieval errors in and around the networks would be the same.*

Continuing with our ''standardized'' solution process, the location information is extracted from the components of $\mathbf{h}$ as

$$\varphi^* = \tan^{-1}\left(\frac{h_3}{h_1}\cos\lambda^*\right), \qquad \lambda^* = \tan^{-1}\left(\frac{h_2}{h_1}\right). \quad (14)$$

By inspecting the standard Euler angle transformations between the coordinate system ($\hat{\mathbf{u}}$, $\hat{\mathbf{v}}$, $\hat{\mathbf{w}}$) and ($\hat{\mathbf{u}}^*$, $\hat{\mathbf{v}}^*$, $\hat{\mathbf{w}}^*$), the source location (φ, λ) relative to the prime meridian and equator can be written in terms of (φ^*, λ^*). With the aid of (9), the final analytic (''LS method'') solution is

$$\varphi = \sin^{-1}(K_{13}\cos\varphi^*\cos\lambda^* + \cos\varphi_1 \sin\varphi^*),$$

$$\lambda = \tan^{-1}\left(\frac{K_{12}\cos\varphi^*\cos\lambda^* + \cos\lambda_1\cos\varphi^*\sin\lambda^* - K_{13}\sin\lambda_1\sin\varphi^*}{K_{11}\cos\varphi^*\cos\lambda^* - \sin\lambda_1\cos\varphi^*\sin\lambda^* - K_{13}\cos\lambda_1\sin\varphi^*}\right), \qquad T = T_1 - \frac{r}{c}\cos^{-1}(\cos\varphi^*\cos\lambda^*), \quad (15)$$

where T_1 is the absolute time (e.g., in GPS seconds) that site 1 is excited by the lightning radio ground wave. Note that the principal values of the inverse cosine function are used, that is, $0 \leq \cos^{-1}(\cos\varphi^* \cos\lambda^*) \leq \pi$, $-\pi/2 < \lambda^* < \pi/2$, $-\pi/2 < \varphi^* < \pi/2$, and T is the absolute time-of-occurrence of the lightning ground wave emission, where $T < T_1$.

We end this section by surveying some mathematical nuances associated with inverting (6) and (11). Since in (6) each component of **f** is divided by $\sin(ct/r)$, the convention $t_1 \equiv 0$ implies that the values of $t = -m\pi r/c$, $m = 0, 1, 2, \ldots$ will produce values of **f** (as well as **h**) that are undefined. That is, **f** is undefined when $m = 0$ (the ground flash strikes site 1), and $m = 1$ (the flash strikes a distance $ct = \pi r \cong 20\,000$ km away from site 1). If this is undesirable to the experimenter, the singularities can be shifted by dividing (5) by $\cos(ct/r)$ rather than $\sin(ct/r)$. In this case, the ''new **g** vector'' would have elements $\cos(ct_i/r)$, and the ''new **K** matrix'' would be identical to the old except that each element of the fourth column would change to $-\sin(ct_i/r)$. The singularities in the ''new **f**'' now satisfy the condition $\cos(ct/r) = 0$, or $t = -m\pi r/(2c)$, $m = 1, 3, 5, \ldots$. This means that the new **f** vector is undefined for sources a distance $ct = \pi r/2 \cong 10\,000$ km away from site 1, but a singularity no longer occurs for ground flashes that strike site 1. However, this shift is not beneficial when the mean sensor baseline is small and the lightning is close to the network. In this case, the fourth column of the new **K** matrix is nearly a zero vector. This means that the new **K** matrix is ill-conditioned, and attempting to invert it would lead to excessive magnification of timing data errors.

Finally, we make mention of the fact that if a ground flash did strike site 1, the experimenter would in fact have ''located'' the lightning and would most assuredly be more concerned about equipment repairs rather than mathematical intractabilities. In this sense, division of (5) by $\sin(ct/r)$ is preferable over division by $\cos(ct/r)$, since the former approach places the singularity twice as far away from site 1.

3. LS method tests and comparisons

In order to test and compare the LS method results provided in (15) with the earlier LP method, it is first assumed that all sources and sensors are located on the surface of a spherical earth. A known source location is selected, and the true (spherical) arrival times at each sensor due to the source are generated. Simulated measurements are produced by adding uniform random errors to the computed arrival times. Next, the simulated measurements are analyzed with the LS method, and the retrieved solution is compared with the known source to compute the location retrieval error. This process is repeated several times at each known source location to generate location retrieval error statistics for that location. Other known source locations are similarly tested so that the spatial distribution of location error can be obtained over a particular region.

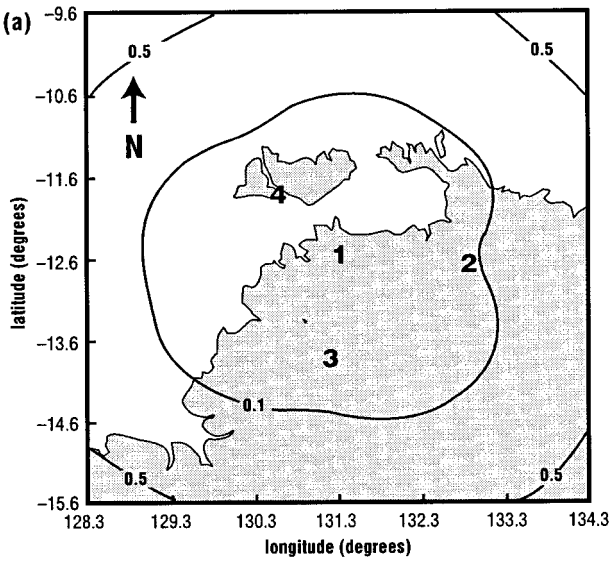

FIG. 2. Lightning location retrieval errors (in km) from a flat-earth retrieval scheme (LP method) assuming no measurement timing errors [adapted from Koshak et al. (2000)]. These results are inferior to the spherical-earth scheme (LS method), which produced retrieval errors below 20 cm.

As in the study by Koshak et al. (2000), four ALDF sites in the region of Darwin, Australia, have been considered. These sites were used as part of the Maritime Continent Thunderstorm Experiment (MCTEX) described in Keenan et al. (1994, 1996). The known (computer-generated) lightning source locations were defined on a grid that had a resolution of 0.02° in latitude and longitude and that spanned a 6° × 6° analysis region.

Before adding random errors to the arrival times, a single known source at each grid location was analyzed with the LS method using the exact (error free) values of t_i. This was done to check the basic mathematical validity of the LS method. Once again, we emphasize the fact that the arrival times were computed assuming the earth was a perfect sphere; that is, the arrival time is the great circle distance between the known source and the sensor, divided by the speed of light. As expected, the LS method performed quite well. Location retrieval errors for the entire 6° × 6° region were below 20 cm. This is substantially less than the retrieval errors found in the LP method described in Koshak et al. (2000) and provided in Fig. 2. Here, the LP method cannot exactly retrieve source locations because arrival times (and magnetic bearings) are formulated on a flat earth surface.

In the second test, 100 retrievals at each grid location were considered. For each of the 100 retrievals, a distinct error (chosen from a uniform random distribution) was added to each of the four arrival times. Figure 3 shows the retrieved location errors for the LP and LS methods when the uniform random distribution had er-

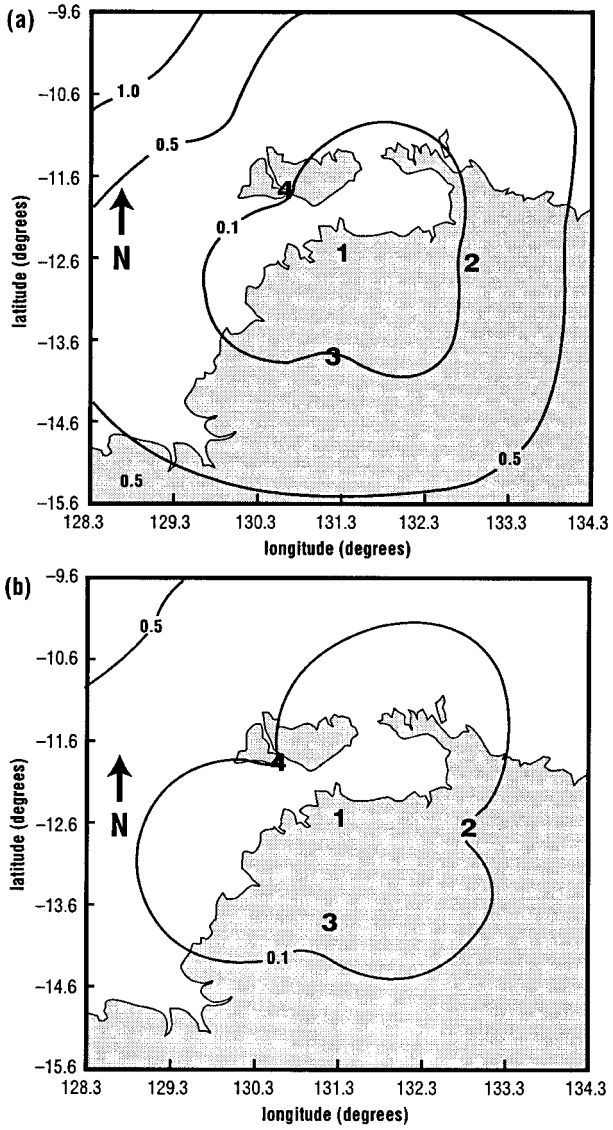

FIG. 3. Lightning location retrieval errors (in km) when a random error between ±100 ns is added to the simulated arrival time data: (a) LP method and (b) LS method.

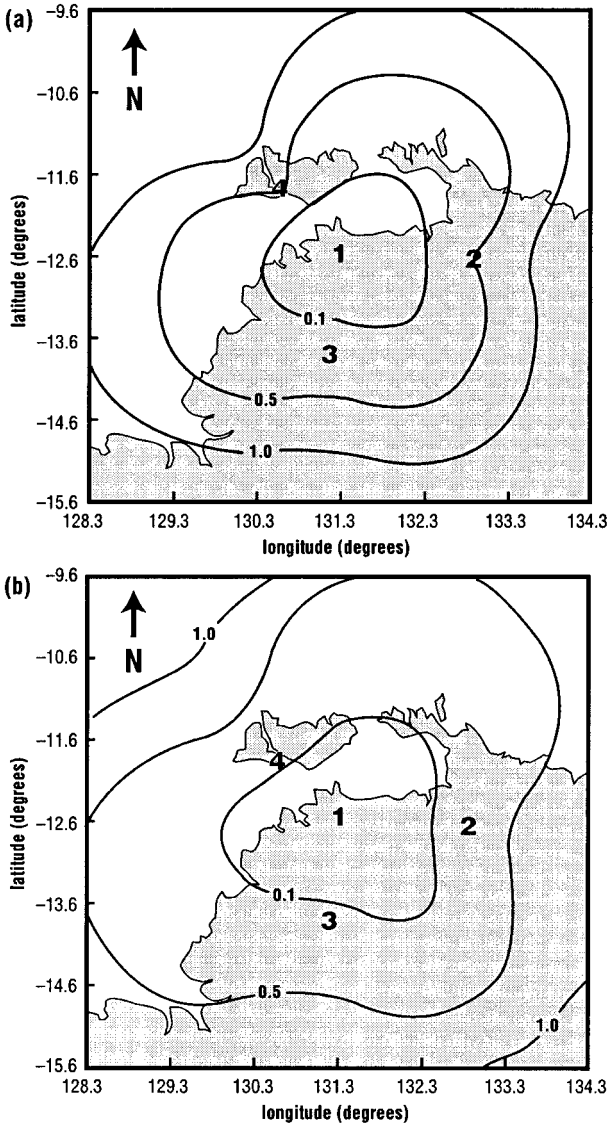

FIG. 4. Lightning location retrieval errors (in km) when a random error between ±300 ns is added to the simulated arrival time data: (a) LP method and (b) LS method.

ror limits of ±100 ns. The mean retrieval error of the 100 trials is plotted for each grid location across the analysis region. Again, the LP retrieval errors (Fig. 3a) are larger than the LS retrieval errors (Fig. 3b) for distant sources. Figure 4 shows how well each method performs when the simulated measurement errors vary between ±300 ns.

In general, we have found that the more distant the lightning source, the more the LS method outperforms the LP method, since earth sphericity effects (such as those shown in Fig. 2) become increasingly important. However, for the relatively small 6° × 6° region, the effects of timing errors (e.g., ±100 and ±300 ns) are more significant than the effects of earth sphericity, and the LP method performs almost as well as the LS method. In the following section, we will consider a much larger analysis region and more distant lightning sources to determine the effects of oblate earth curvature on location retrieval accuracy.

4. IO method for oblate spheroidal earth

By perturbing the spherical earth model results of the LS method described in section 2, we obtain immediate extensions to an oblate spheroid. In so doing, the perturbation provides a quantitative means for directly assessing oblate effects. The set of perturbed equations are solved by a Newton-type iteration, and we call the approach an iterative oblate (IO) method. Such iterative procedures have excellent convergence properties if a

good initial guess is available. Since the earth is very nearly a sphere, the LS method provides an excellent initial guess of lightning source location.

Letting $S_i(\varphi, \lambda)$ denote the distance along a geodesic of an oblate spheroidal earth between the ith TOA sensor and a lightning located at latitude φ and longitude λ, we may write the transit equation as

$$S_i(\varphi, \lambda) = c(t_i - t), \tag{16}$$

where c is the speed of the ground wave and t is the time-of-occurrence of the cloud-to-ground discharge. Next, we use the results of the LS method provided in (15) to obtain the initial estimates $(\varphi^{(0)}, \lambda^{(0)}, t^{(0)})$ to the true lightning source parameters (φ, λ, t). Denoting the errors in these estimates as $\delta\varphi \equiv \varphi - \varphi^{(0)}$, $\delta\lambda \equiv \lambda - \lambda^{(0)}$, and $\delta t = t - t^{(0)}$, we may rewrite (16) as

$$S_i(\varphi^{(0)} + \delta\varphi, \lambda^{(0)} + \delta\lambda) = c[t_i - (t^{(0)} + \delta t)]. \tag{17}$$

Expanding the left-hand side of (17) in a Taylor series and neglecting higher-order terms gives the approximative set of equations

$$S_i(\varphi^{(0)}, \lambda^{(0)}) + \left.\frac{\partial S_i}{\partial \varphi}\right|_{(\varphi^{(0)}, \lambda^{(0)})} \delta\varphi + \left.\frac{\partial S_i}{\partial \lambda}\right|_{(\varphi^{(0)}, \lambda^{(0)})} \delta\lambda \cong c[t_i - (t^{(0)} + \delta t)], \tag{18}$$

for sensors $i = 1, 2, 3, 4$. Hence, (18) constitutes a (4×3) linear system of equations in the three unknowns $(\delta\varphi, \delta\lambda, \delta t)$. As such, it is an overdetermined system that can be solved in a least squares sense. Because we have truncated the Taylor series, (18) is a set of approximative equations. Hence, inversion of the (4×3) system provides only approximations to the exact corrections $(\delta\varphi, \delta\lambda, \delta t)$. Nonetheless, the three approximative corrections, which we denote as $(\delta\varphi^{(0)}, \delta\lambda^{(0)}, \delta t^{(0)})$, improve upon the initial LS method estimates $(\varphi^{(0)}, \lambda^{(0)}, t^{(0)})$. Furthermore, we need not stop after one iterative update of the solution but can carry out a total of $N = n + 1$ iterations. With these ideas in mind, our (4×3) system can be written as

$$\begin{bmatrix} \partial_\varphi S_{1n} & \partial_\lambda S_{1n} & c \\ \partial_\varphi S_{2n} & \partial_\lambda S_{2n} & c \\ \partial_\varphi S_{3n} & \partial_\lambda S_{3n} & c \\ \partial_\varphi S_{4n} & \partial_\lambda S_{4n} & c \end{bmatrix} \begin{bmatrix} \delta\varphi^{(n)} \\ \delta\lambda^{(n)} \\ \delta t^{(n)} \end{bmatrix} = \begin{bmatrix} c(t_1 - t^{(n)}) - S_1(\varphi^{(n)}, \lambda^{(n)}) \\ c(t_2 - t^{(n)}) - S_2(\varphi^{(n)}, \lambda^{(n)}) \\ c(t_3 - t^{(n)}) - S_3(\varphi^{(n)}, \lambda^{(n)}) \\ c(t_4 - t^{(n)}) - S_4(\varphi^{(n)}, \lambda^{(n)}) \end{bmatrix}, \tag{19}$$

where $\partial_\omega S_{in}$ is shorthand notation for $\partial S_i/\partial\omega$ evaluated at $(\varphi^{(n)}, \lambda^{(n)})$, with $\omega = \varphi, \lambda$. Expressing the matrix as $\mathbf{A}_n$, the column vector on the left as $\mathbf{x}_n$, and the column vector on the right-hand side (rhs) as $\mathbf{y}_n$, we can write (19) as

$$\mathbf{A}_n \mathbf{x}_n = \mathbf{y}_n. \tag{20}$$

Unlike the approximative form given in (18), this (4×3) linear system is exact. The least squares iterative update of the oblate earth solution defined by $\mathbf{b}_{n+1} = (\varphi^{(n+1)}, \lambda^{(n+1)}, t^{(n+1)})$ can now be written as

$$\mathbf{b}_{n+1} = \mathbf{b}_n + (\tilde{\mathbf{A}}_n \mathbf{A}_n)^{-1} \tilde{\mathbf{A}}_n \mathbf{y}_n. \tag{21}$$

Iteration is continued until $|\mathbf{x}_n| = |(\delta\varphi^{(n)}, \delta\lambda^{(n)}, \delta t^{(n)})|$ is less than a prescribed tolerance; the last term in (21) is of course the least squares solution of (20) for $\mathbf{x}_n$. Exact representations for the derivatives in $\mathbf{A}_n$ may be used, but we have used simple secant-type approximations. For example, one can use $\partial S_i/\partial\lambda \cong [S_i(\varphi, \lambda + 0.0025°) - S_i(\varphi, \lambda - 0.0025°)]/0.005°$. In either case, the derivatives of S_i are well behaved.

Explicit expressions for the needed geodesic distances $S_i(\varphi, \lambda)$ are obtainable using variational calculus on an oblate spheroid (see the appendix). In this study, we have opted to use the computationally efficient forms provided in Sodano (1965; appendix A), where geodesic distances are computed to within a few centimeters accuracy.

5. Importance of oblate spheroidal corrections

The IO method described in section 4 converges rapidly and is highly accurate when error-free arrival times are analyzed. Consider a fictitious (high gain) network of four stations located at Chattanooga, Tennessee (35.06°, −85.30°); Florence, Alabama (34.79°, −87.67°); Huntsville, Alabama (34.73°, −86.59°); and Birmingham, Alabama (33.52°, −86.79°). If a lightning event occurs in Chicago, Illinois (41.89°, −87.65°), the distances to the four stations along geodesics are 785.319 770 339, 788.125 066 758, 800.148 006 314, and 932.073 066 608 km, respectively. The lightning radio wave will arrive at Chattanooga first, followed by Florence, Huntsville, and Birmingham. If we say it arrives at Chattanooga at 0 μs, then it arrives at the other three sites at 9.357 461 62 μs, 49.461 671 17 μs, and 489.516 304 88 μs, respectively. The LS method solution is (φ = 41.890 763 66°, λ = −87.649 892 06°, t = −2620.254 395 μs). In this case, the distance between the true source location and retrieved location is about 85.29 m, and the error in the retrieved time-of-occurrence is about 0.71 μs. Here, the effects of measurement and propagation errors are not considered in this purely mathematical test. In addition, the 1984 World Geodetic System Earth Ellipsoid (WGS-84 Ellipsoid), having semimajor (6378.137 km) and semiminor (6356.752 314 2 km) axes, were taken to be absolutely accurate.

Just one iteration of the IO method provides the improved solution (41.889 999 913°, −87.650 000 011 2°, −2619.544 754 μs). The distance error is now only about 9.7 mm, and the time-of-occurrence error is 32.4 ps.

To further examine the importance of oblate effects, we consider the 4-station Darwin network discussed earlier but view a much larger (90° × 90°) region centered about the central ALDF site (site 1). We compute both

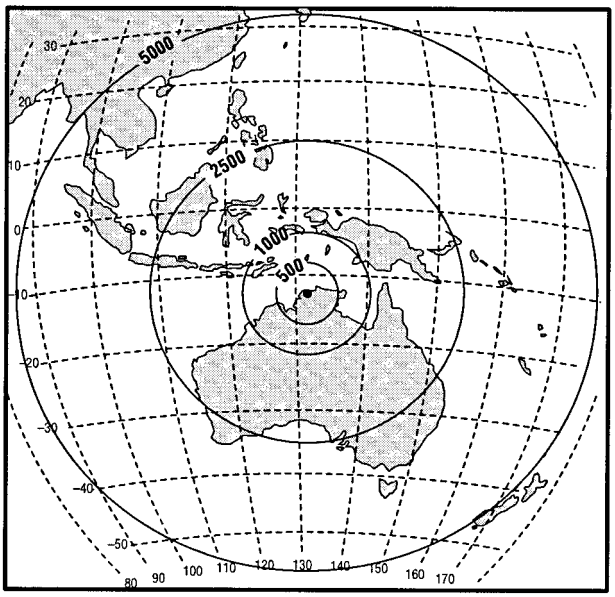

FIG. 5. The spatial distribution of the geodesic distance (in km) from site 1 assuming an oblate spheroidal earth geometry. The distribution was obtained by using a computationally efficient noniterative method introduced by Sodano (1965, appendix A).

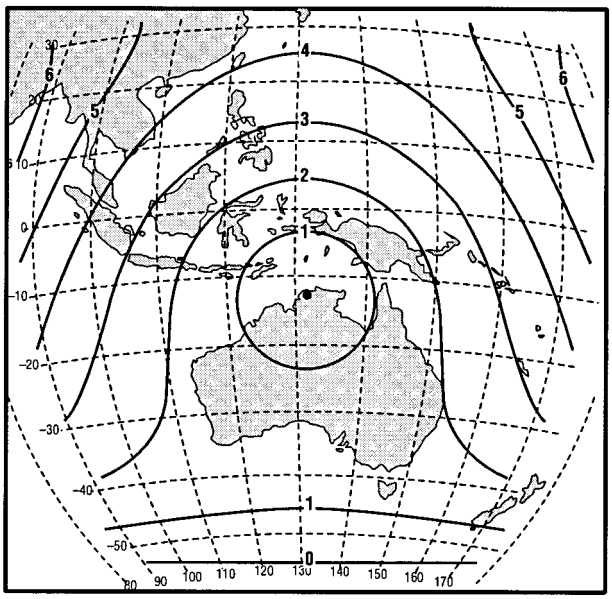

FIG. 6. The spatial distribution of the difference (oblate-earth distance minus spherical-earth distance, in km) to site 1.

the spherical earth great circle distance and the oblate earth geodesic distance between site 1 and (several) fictitious lightning source locations. The source locations are defined on a grid that spans the entire ($90° \times 90°$) area and that has a grid resolution of 1°. In other words, we computed the spatial distribution of the spherical and oblate geodesic distances from site 1.

The oblate distances to site 1 are shown in Fig. 5. As expected, a concentric geometry is obtained, that is, as one moves farther from site 1, the geodesic distance increases. At this map scale, the corresponding distribution of spherical distances to site 1 looks essentially the same. To emphasize the discrepancy between the two, the difference (oblate distance minus spherical distance) is provided in Fig. 6. Dividing this distribution by the speed of light, *c*, indicates how the arrival times would differ due solely to earth geometry differences.

However, these results do not provide specific information as to how oblate effects directly affect a source location retrieval. To determine this, we have analyzed each fictitious source from the grid using the LS method described in section 2. When spherical earth (great circle) arrival times are used, the LS method retrieves source location to better than 20 cm. There were no assumed arrival time errors and only minimal computer truncation error, since double precision floating point computations were performed. However, when the LS method is used to analyze the corresponding oblate earth arrival times produced from the same set of fictitious sources (again with no simulated arrival time error), the location retrieval errors shown in Fig. 7 are obtained. Clearly, the penalty for neglecting oblate effects within the LS method is nontrivial. The maximum retrieval error in Fig. 7 is 13.70 km.

By comparison, we applied the IO method discussed in section 4 to analyze the same oblate earth arrival times and found that location retrieval errors were below

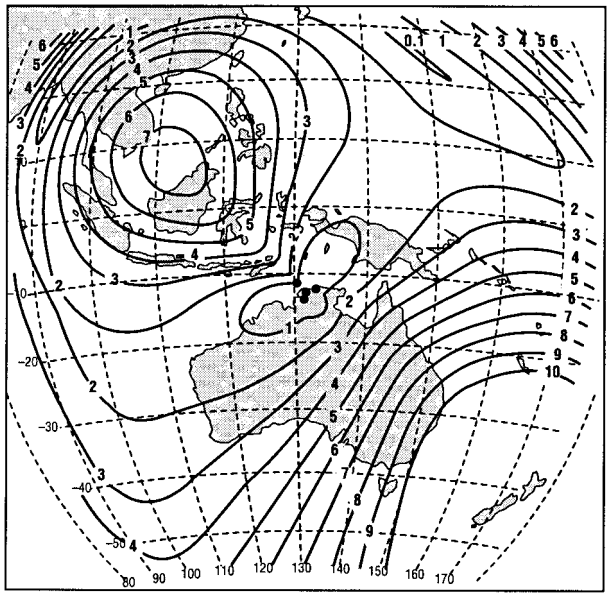

FIG. 7. The spatial distribution of location retrieval errors (in km) obtained from the LS method when simulated arrival times are computed on an oblate earth. No simulated measurement errors were added to the arrival times. Since the LS method assumes a spherical earth geometry, the analysis of oblate-earth arrival times must produce retrieval errors. By comparison, the IO method discussed in section 4 of the text produces location retrieval errors all below 20 cm.

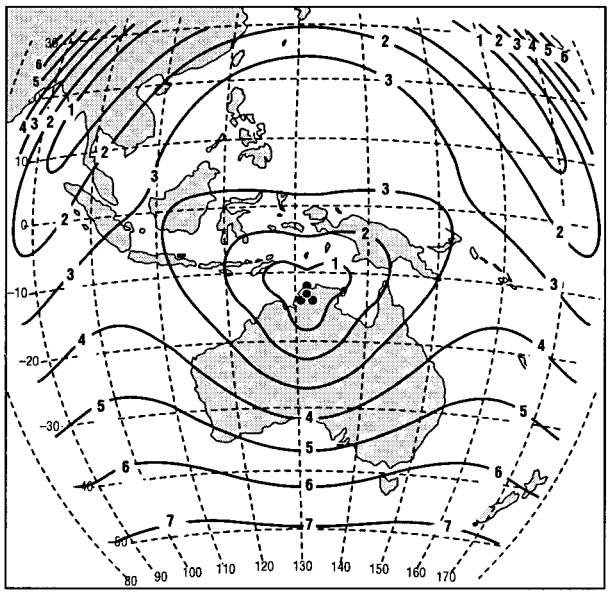

FIG. 8. Same as in Fig. 7 but with a modified and more symmetric network geometry. This plot explicitly shows that network geometry significantly modulates the spatial distribution of location retrieval error. Again, the IO method discussed in section 4 of the text produces location retrieval errors all below 20 cm.

20 cm. Less than five Newton-type iterations per source were used to achieve this retrieval accuracy. In the absence of instrument timing errors, the IO method accurately accounts for all oblate effects.

At this point, one might wonder why the errors in Fig. 7 are not spatially distributed like the difference errors provided in Fig. 6. That is, one might expect location retrieval errors to be largest where the differences plotted in Fig. 6 are greatest. This, however, is not true. In reality, *the sensor network geometry modifies the spatial distribution of retrieval error*. Or, equivalently, the accuracy of the LS solution provided in (15) depends on source location and network geometry. To explicitly show this, we have reanalyzed all the same source locations using a sensor network that is the same typical size as before but that has a perfect symmetry about a north–south line. More specifically, we rotated the old network clockwise about the central site. We then adjusted the locations of the outer sites so that they were each about 111 km from the central site and evenly spaced in azimuth from one another.

The new symmetric network and the new location retrieval errors are provided in Fig. 8. The maximum retrieval error is now only 7.83 km (compared to the 13.70-km value of Fig. 7). Note that many features of the location error distribution in Fig. 7 have rotated clockwise in accordance to the clockwise rotation of the network. Since the new network is more symmetric than the old, the new location error distribution is more symmetric than in Fig. 7. Clearly, the spatial distribution of retrieval errors is intimately tied to network geometry.

Such effects are not unique to this problem. Network geometry was seen to influence flat-earth (LP method) solutions, especially for sources located on outer sensor baselines, where retrieval errors are relatively large (Koshak et al. 2000). Similarly, we see relatively large location errors along the outer sensor baselines in Figs. 7 and 8.

As we have shown, the neglect of earth oblateness in the LS method results in nontrivial location errors. However, it is more realistic to ask the question: *Are oblate effects important in the presence of instrument arrival time errors?* To be complete, one should include *all* errors in this question, not just those due to instrument uncertainties. For example, one could include propagation errors that are related to inhomogeneities in earth surface conductivity, terrain scattering, and any differences in pathlength due to the fact that the radio wave might actually reflect off the ionosphere rather than propagate along the surface. However, inclusion of these errors is beyond the scope of this work.

In order to assess the importance of oblate effects in the presence of instrument timing errors alone, we analyzed 100 sources at each grid location across the (90° $\times$ 90°) region. A random timing error was added to the simulated arrival times so that the mean location retrieval error for the 100 sources at a particular grid location could be computed. This process was repeated for all grid locations in the (90° $\times$ 90°) region to obtain the spatial distribution of location retrieval error.

For illustrative purposes, we began with an unrealistically small ($\pm$10 ns) instrument arrival time error. The error is selected from a uniform random distribution in the interval [$-$10 ns, 10 ns]. The results of the LS and IO methods are provided in Fig. 9. Note that the IO method improves upon the LS method results; however, the improvement is not as pronounced as when exact arrival times were used (i.e., Fig. 7 had errors in excess of 10 km, while the IO method produced errors below 20 cm). Note also that the error pattern in Fig. 9a resembles that in Fig. 7. This means that the effects of timing errors are not large enough to completely obscure (network-geometry modulated) oblate earth effects. The error pattern in Fig. 9b does *not* resemble the error pattern in Fig. 7 because the IO method accounted for oblate effects in the former.

When the random error is increased to $\pm$100 ns, we obtain the location errors shown in Fig. 10. Because of the larger timing error, the oblate earth effects in Fig. 10a are more obscured (i.e., the error pattern in Figs. 9a and 7 are more similar than between Figs. 10a and 7). Furthermore, a comparison between Figs. 10a and 10b indicates that the LS results are better than the IO results for many (but not all) source locations. For sources located where oblate earth effects are large (as judged by Fig. 7), the iterations of the IO method tend to improve LS results. However, where oblate earth effects are small, the iterations tend to worsen the LS results.

Mathematically, instrument timing errors degrade the accuracy of the initial solution estimate afforded by the

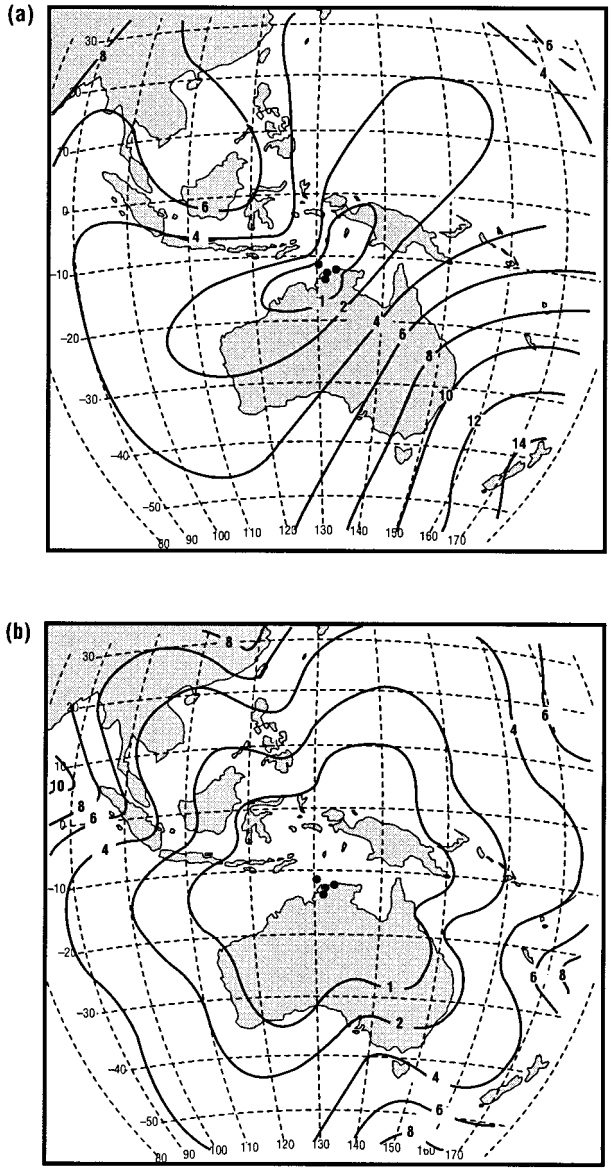

FIG. 9. The spatial distribution of location retrieval errors (in km) assuming an unrealistically small random timing error of ±10 ns using the (a) LS method and (b) IO method. Note that the IO method is an improvement over the LS method.

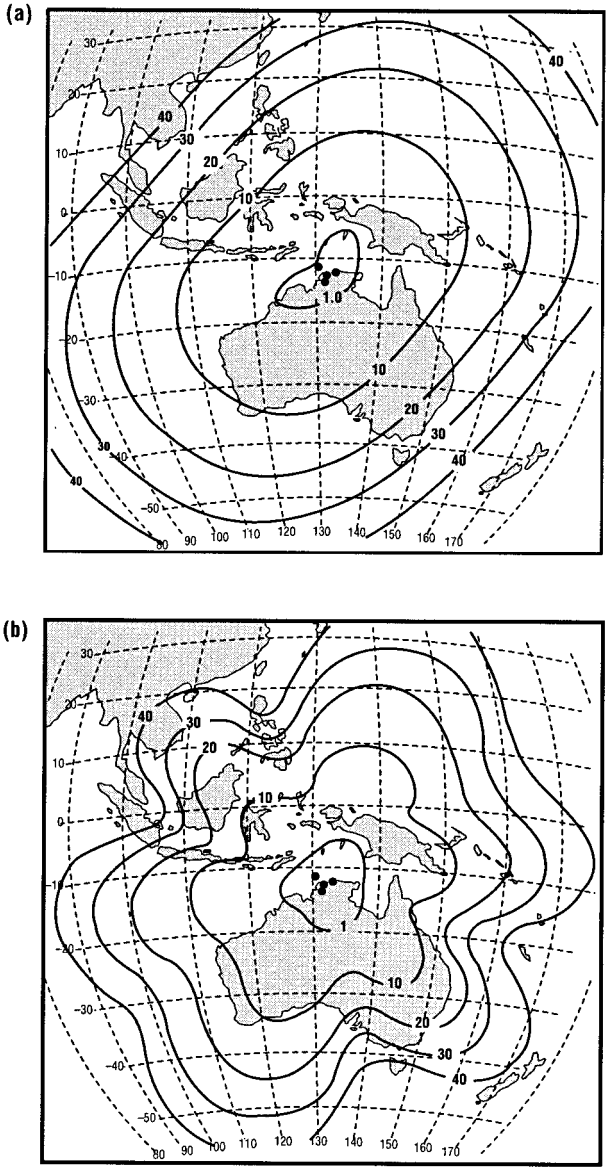

FIG. 10. The spatial distribution of location retrieval errors (in km) assuming a random timing error of ±100 ns using the (a) LS method and (b) IO method. Here, unlike in Fig. 9, the IO method does not improve upon the LS method results for many source locations. This is due to the additional timing error of this simulation.

LS method. In addition, the timing errors add errors to each iterative correction term $(\tilde{\mathbf{A}}_n\mathbf{A}_n)^{-1}\tilde{\mathbf{A}}_n\mathbf{y}_n$ in (21), where $n = 0, 1, 2, 3, 4$. Specifically, (19) shows that the 4-vector $\mathbf{y}_n$ depends directly on arrival time data. Therefore, $\mathbf{y}_n$ in (21) should be replaced with $\mathbf{y}_n + \mathbf{e}_n$ when instrument timing errors are present, where $\mathbf{e}_n$ is an error 4-vector. The error added to each solution iterate is then given by $(\tilde{\mathbf{A}}_n\mathbf{A}_n)^{-1}\tilde{\mathbf{A}}_n\mathbf{e}_n$.

Interestingly, the (3×4) matrix $(\tilde{\mathbf{A}}_n\mathbf{A}_n)^{-1}\tilde{\mathbf{A}}_n$ depends on the location $(\varphi^{(n)}, \lambda^{(n)})$ but not directly on arrival time data. Nonetheless, the mathematical nature of this matrix plays a role in determining how the errors $\mathbf{e}_n$ affect solution accuracy. First, the condition of the matrix $\tilde{\mathbf{A}}_n\mathbf{A}_n$ is important. If it is ill conditioned, it will have small eigenvalues, and the elements of $(\tilde{\mathbf{A}}_n\mathbf{A}_n)^{-1}$ will be large, thereby leading to large solution errors. Fortunately, in all of our computer simulations, we saw no evidence of an ill-conditioned nature in $\tilde{\mathbf{A}}_n\mathbf{A}_n$. Second, the matrix $(\tilde{\mathbf{A}}_n\mathbf{A}_n)^{-1}\tilde{\mathbf{A}}_n$ defines a *linear transformation* that maps a 4-vector $\mathbf{e}_n$ into a 3-vector $(\mathbf{d}_n)$. We may express this mapping as $\mathbf{d}_n = \mathbf{M}(\varphi^{(n)}, \lambda^{(n)})\mathbf{e}_n$, where $\mathbf{M}(\varphi^{(n)}, \lambda^{(n)}) \equiv (\tilde{\mathbf{A}}_n\mathbf{A}_n)^{-1}\tilde{\mathbf{A}}_n$. Given n, the set of error vectors satisfying the property $\mathbf{M}(\varphi^{(n)}, \lambda^{(n)})\mathbf{e}_n = \mathbf{0}$ is called the *nullspace* of the linear transformation. Since this homogeneous system of linear equations has more

TABLE 1. A detailed look at the LS and IO method results for a source located at 10° latitude and 150° longitude when instrument timing errors are 0 and ± 100 ns. The WGS-84 earth ellipsoid defined in section 5 was used. The italicized numbers (shown for $n = 0$) are the retrieved locations produced by the LS method, and the bold numbers are the final retrieved locations produced by the IO method. Full double precision floating point numbers are not provided here but were used in all computer calculations. For no timing error, the LS method has 1.332 km location error compared with 0 km location error for the IO method. For ±100-ns timing error, the respective location errors are 19.357 km and 54.536 km. Because oblate earth effects are relatively small at this source location, the IO method does not improve upon the LS method when timing errors are added.

Iteration (n)	$\varphi^{(n)}$	$\delta\rho^{(n)}$	$\lambda^{(n)}$	$\delta\lambda^{(n)}$
0-ns timing error				
0	*9.989495562*	0.010498551	*149.994173556*	0.005822359
1	9.999994113	0.000005887	149.999995916	0.000004084
2	10.000000000	0.000000000	150.000000000	0.000000000
3	10.000000000	0.000000000	150.000000000	0.000000000
4	10.000000000	0.000000000	150.000000000	0.000000000
—	**10.000000000**	—	**150.000000000**	—
±100-ns timing error				
0	*9.863585935*	−0.243960212	*149.890496401*	−0.209285651
1	9.619625723	0.002467566	149.681210750	0.002321537
2	9.622093288	0.000000472	149.683532287	0.000000448
3	9.622093760	0.000000000	149.683532735	0.000000000
4	9.622093760	0.000000000	149.683532735	0.000000000
—	**9.622093760**	—	**149.683532735**	—

unknowns (four) than equations (three), it has infinitely many solutions in addition to the trivial solution ($\mathbf{e}_n = \mathbf{0}$). A parametric solution of the homogeneous system (see Anton 1984, chap. 1) provides the type (i.e., the mathematical form) of error vectors that would be nullified by $\mathbf{M}$. Even though these error vectors mathematically exist, it is unlikely that an actual error vector from a real data inversion problem would be of the exact form required for complete nullification. Nonetheless, it is so noted that error nullification is possible.

To further demonstrate the nature of the IO method, we have collected iterative results in tabular form for two specific source locations; one source location is associated with small oblate effects and the other with large. The relative strength of oblate effects, ''small'' or ''large,'' are determined from Fig. 7. Table 1 shows results for a source located at $(\varphi, \lambda) = (10°, 150°)$ for both 0 and ±100-ns instrument uncertainties. Figure 7 indicates that oblate effects are relatively small for this location. As indicated above, the IO method does an excellent job of improving LS method results when there are no instrument timing errors. The LS method had a location retrieval error of 1.332 km, but the IO method had effectively 0 km of error. However, with ±100-ns timing error, the LS method produces an error of 19.357 km, and the IO method degrades this result to 54.536 km. Table 2 shows results for a source located at $(\varphi, \lambda) = (10°, 110°)$, where oblate effects are large. Once again, for no instrument timing error, the IO method has 0-km retrieval error compared with a 7.220-km LS method retreival error (the LS results are particularly poor here because oblate effects are large). In the pres-

TABLE 2. Same as in Table 1 except for a source located at 10° latitude and 110° longitude. For no timing error, the LS method has a 7.220-km location error compared with 0-km location error for the IO method. For ±100-ns timing error, the respective location errors are 47.621 km and 5.113 km. Because oblate earth effects are relatively large at this location, the IO method improves upon the LS method.

Iteration (n)	$\varphi^{(n)}$	$\delta\rho^{(n)}$	$\lambda^{(n)}$	$\delta\lambda^{(n)}$
0-ns timing error				
0	*9.950425087*	0.049508407	*110.042472365*	−0.042408869
1	9.999933495	0.000066505	110.000063496	−0.000063495
2	10.000000000	0.000000000	110.000000000	0.000000000
3	10.000000000	0.000000000	110.000000000	0.000000000
4	10.000000000	0.000000000	110.000000000	0.000000000
—	**10.000000000**	—	**110.000000000**	—
±100-ns timing error				
0	*9.683918714*	0.276701673	*110.292633112*	−0.261296833
1	9.960620387	0.002869349	110.031336279	−0.003028444
2	9.963489736	0.000000046	110.028307835	−0.000000141
3	9.963489782	0.000000000	110.028307693	0.000000000
4	9.963489781	0.000000002	110.028307694	−0.000000002
—	**9.963489783**	—	**110.028307692**	—

ence of a ±100-ns timing error, the LS method retrieval error jumps to 47.621 km, but the IO method had a retrieval error of only 5.113 km.

In summary, attempting to correct for oblate earth effects is not always prudent. One must first consider network geometry, the magnitude of instrument (and other propagation) errors, and source location. When network-modulated oblate earth effects are small relative to the adverse effects of instrument timing errors, the LS method retrieval error plus the accumulated errors due to IO method iterations exceed the LS method retrieval error. In these cases, application of the IO method degrades the basic LS solution. Convergence is obtained with few (e.g., 5) Newton-type iterations, but the convergence is toward a false solution point. When network-modulated oblate earth effects are large relative to the effects of timing errors, the IO method improves LS results.

6. Results for Darwin and Brazil TOA networks

There is no overall advantage in applying the iterative update scheme in (21) when (more realistic) timing errors of ±300 ns are assumed. In this case, the large timing errors make it difficult to correct for even reasonably large oblate effects. However, the LS method still provides a reasonably accurate solution. Figure 11 shows the LS method location retrieval error for two different measurement networks when a timing error of ±300 ns is assumed. Figure 11a is for the familiar Darwin network that we considered in section 5 above, and Fig. 11b is for a new network located in Brazil. Like the Darwin network, the Brazil network consists of four ALDF sensors that were developed to support ground-validation activities of the OTD and LIS space-borne lightning detectors. The Brazil network was recently installed and is currently operational.

It is interesting that the larger sensor baseline of the Brazil network significantly improves the location accuracy of distant sources. The 10-km error contour in Fig. 11b (i.e., the contour that approximately matches the characteristic resolution of the OTD low earth orbiting lightning detector) encompasses a significant fraction of the South American continent. However, the 10-km error contour of Fig. 11a bounds a much smaller area. The maximum location retrieval error across the entire (90° × 90°) region of Fig. 11a was 291.8 km, but it was only 82.3 km in the (90° × 90°) region of Fig. 11b.

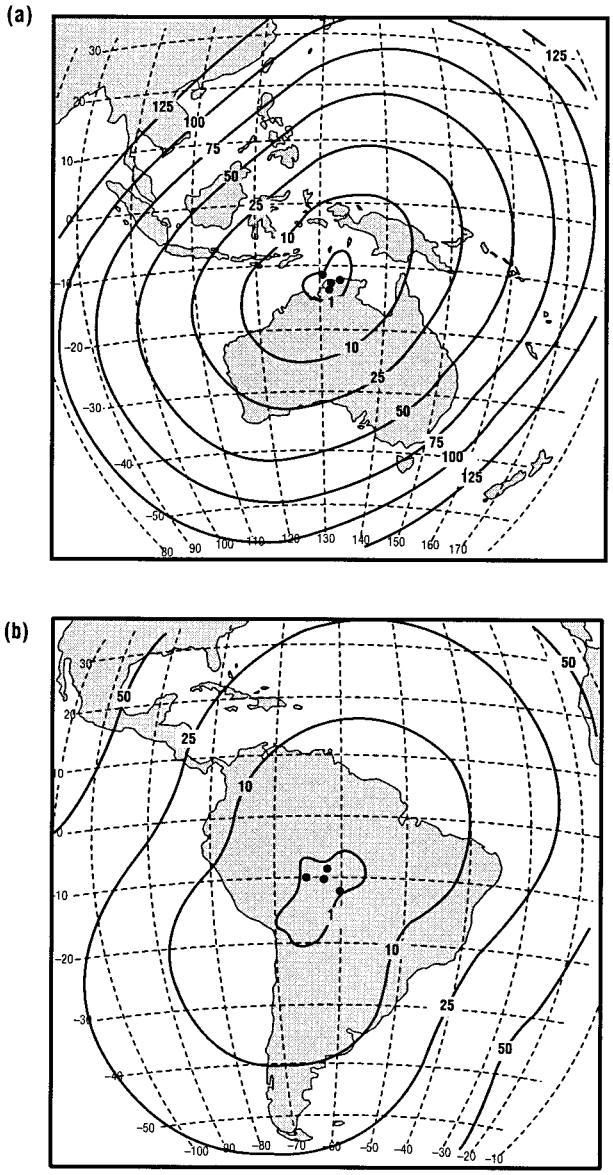

FIG. 11. The location retrieval error (in km) assuming an instrument timing error of ±300 ns for the (a) Darwin network (b) Brazil network.

7. Summary

A method was introduced to retrieve the location and time-of-occurrence of ground flashes using a network of four or more TOA sensors. The mathematical solution is derived in spherical coordinates and fully accounts for earth sphericity. Solving for the unknown lightning source is done by simply inverting (12) and then applying (14) and (15). The method is computationally quick and can be implemented using just a few lines of computer code. With assumed instrument timing errors of ±300 ns, overall lightning location retrieval error from the method is within tens of kilometers. This is small given the large (90° latitude × 90° longitude) region and relatively short sensor baselines that we have considered. Location errors less than 10 km are also evident over a large subregion. Because earth curvature is accounted for, the spherical earth method is more accurate than earlier flat earth methods introduced in Koshak et al. (2000). However, if instrument arrival time errors are sufficiently large and/or the analysis region

sufficiently small, no appreciable difference in the results of the two methods are seen.

We emphasize that the spherical earth method (LS method) represents an algebraic solution. Hence, we do not need to employ nonlinear numerical methods to obtain an answer. For example, we do not need to perform a computer search to determine the solution parameters that minimize a nonlinear χ^2 function. Such a search can lead to erroneous solutions if the presence of measurement errors produce multiple relative minima in the χ^2 surface. Currently, arrival time and magnetic bearing data obtained from the National Lightning Detection Network (NLDN) are simultaneously analyzed by minimizing a χ^2 function (Cummins et al. 1995, 1998). If magnetic-bearing data can be implemented into our spherical formalism, perhaps by considering the analytic work of Orville (1987), then minimization of a χ^2 function would prove to be unnecessary.

Finally, we have extended our spherical earth approach to account for the effects of earth oblateness using a simple Newton-type iterative approach. Retrieval errors on an oblate surface using this approach are below 20 cm when exact (error free) simulated arrival time data are used. To the best of our knowledge, this has not been previously accomplished. For example, the χ^2 approach used for the NLDN uses a best-fit sphere approximation to partially account for oblate effects (K. L. Cummins 1999, personal communication). Furthermore, we have shown that small amounts of instrument timing error ($\sim$100 ns) can prevent Newton iterations from correcting for small ($<$5 km) oblate effects. In fact, the Newton iterations can actually degrade the LS results. In effect, we have demonstrated that the ''cure'' (IO method) is worse than the ''affliction'' (oblate effects) when the effects of instrument uncertainties are large in comparison to (network-modulated) oblate earth effects. Nonetheless, the IO method works exceptionally well when instrument error is greatly reduced and regions possessing large oblate effects are considered.

Given time, improvements in technology will reduce instrument uncertainties, thereby making the IO method progressively attractive. However, even if timing errors could be completely eliminated, radio wave propagation errors (such as those mentioned in section 5) would need to be considered relative to oblate effects. Taking all of this into consideration, we have employed the LS method and a present-day instrument uncertainty of $\pm$300 ns to determine the location retrieval error over a large region for two different TOA networks. We found that the TOA networks could ground-truth OTD/LIS space sensors over a large (continent-scale) area and that larger baseline networks offer greater area ground-truth coverage.

In the future, the authors intend to use the LS and IO methods to analyze a wide range of thunderstorms and to relate the results to other independent datasets such as OTD, LIS, radar, Lightning Detection and Ranging (LDAR), and data from the North American Lightning Detection Network (NALDN) discussed in Cummins et al. (1999). Again, more elegant solutions that incorporate magnetic bearing data but that still retain a linear matrix formulation will be investigated.

Acknowledgments. We appreciate the work of Susan Burrer in completing the final form of this manuscript and the work of Janine Roskowski for her help in preparing the final figures. The authors wish to thank Dr. Richard Blakeslee of NASA Marshall Space Flight Center (MSFC) for his practical insights regarding the Darwin and Brazil ALDF networks and Prof. E. Philip Krider of the University of Arizona for his help in scientific literature searches. The work of coauthor (Solakiewicz) was supported by the 1999 NASA/MSFC Summer Faculty Program. Finally, we are grateful for the support of this research by Dr. Ramesh Kakar of NASA Headquarters under task #622-29-40, the NASA Earth Observing System (EOS) Program under Task 229-71-46, and the NASA Headquarters Validation Program NRA-97-MTPE-03.

APPENDIX

Variational Method for Verifying Sodano's Geodesic Distance Calculations

In order to verify the accuracy of the computationally efficient results of Sodano (1965, appendix A), expressions are needed for the distances $S_i(\varphi, \lambda)$. Geodesics on a sphere are great circles, and geodesics on an oblate spheroid may be calculated using the calculus of variations. Oblate spheroidal coordinates (ξ, η, λ) are related to Cartesian coordinates (x, y, z) by

$$x = \gamma \cosh\xi \cos\eta \cos\lambda, \qquad y = \gamma \cosh\xi \cos\eta \sin\lambda,$$
$$z = \gamma \sinh\xi \sin\eta, \tag{A1}$$

where $\xi > 0$, $-\pi/2 \le \eta \le \pi/2$, and $0 \le \lambda < 2\pi$. Here, γ is a constant, and we will be working on a constant oblate spheroidal surface, ξ. The products $\gamma \cosh\xi = A$ and $\gamma \sinh\xi = B$ will be taken to be the mean equatorial radius and polar radius of the earth, respectively. The transformation between spherical latitude φ and oblate spheroidal latitude η is

$$\tan\eta = \frac{A}{B} \tan\varphi. \tag{A2}$$

Spherical and oblate longitudes are identical and are denoted by the variable λ.

The arc length of a geodesic on the surface of an oblate spheroid may be represented by the integral

$$S = \int_{\lambda_1}^{\lambda_2} d\lambda \sqrt{P + 2Q\frac{d\eta}{d\lambda} + R\left(\frac{d\eta}{d\lambda}\right)^2}, \tag{A3}$$

where λ_1 and λ_2 are longitude coordinates of the endpoints of the arc, and we have the functions

$$P = \left(\frac{\partial x}{\partial \lambda}\right)^2 + \left(\frac{\partial y}{\partial \lambda}\right)^2 + \left(\frac{\partial z}{\partial \lambda}\right)^2 = A^2 \cos^2\eta,$$

$$Q = \frac{\partial x}{\partial \lambda}\frac{\partial x}{\partial \eta} + \frac{\partial y}{\partial \lambda}\frac{\partial y}{\partial \eta} + \frac{\partial z}{\partial \lambda}\frac{\partial z}{\partial \eta} = 0,$$

$$R = \left(\frac{\partial x}{\partial \eta}\right)^2 + \left(\frac{\partial y}{\partial \eta}\right)^2 + \left(\frac{\partial z}{\partial \eta}\right)^2 = A^2 \sin^2\eta + B^2 \cos^2\eta. \quad \text{(A4)}$$

The Euler–Lagrange equation for this problem takes on the usual form

$$\frac{\partial f}{\partial \eta} - \frac{d}{d\lambda}\left(\frac{\partial f}{\partial \eta'}\right) = 0, \quad \text{(A5)}$$

where $f = \sqrt{P + 2Q\eta' + R(\eta')^2}$. The derivative in the integrand of (A3) can be written as

$$\frac{d\eta}{d\lambda} = C\sqrt{\frac{R}{P^2 - CP}}, \quad \text{(A6)}$$

where C is a constant that is determined by a pair of points that the geodesic passes through. If η changes monotonically with λ, then C is the solution to

$$\lambda_2 - \lambda_1 = \frac{C}{A}\int_{\eta_1}^{\eta_2} d\eta \sqrt{\frac{A^2 \sin^2\eta + B^2 \cos^2\eta}{A^2 \cos^2\eta - C^2}}\,\sec\eta. \quad \text{(A7)}$$

Here, C is bounded by $A\cos(\min[|\eta_1|, |\eta_2|])$. If (A7) cannot be satisfied, then η does not change monotonically with λ. This situation occurs, for example, if one wants to get from a point in the United States to a point in Asia with the same latitude. One would make a northward excursion first. In such cases, C would be chosen to satisfy

$$\lambda_2 - \lambda_1 = \frac{C}{A}\sum_{j=1}^{2}\int_{\eta_j}^{\cos^{-1}C/A} d\eta \sqrt{\frac{A^2 \sin^2\eta + B^2 \cos^2\eta}{A^2 \cos^2\eta - C^2}}\,\sec\eta. \quad \text{(A8)}$$

The equations for obtaining C are transcendental, and they must be solved numerically. A Newton–Rhapson or secant method can be applied. Once C has been determined to sufficient accuracy, arc length is determined from one of

$$S = \sqrt{A^2 - B^2}\int_{\nu_1}^{\nu_2} dt \sqrt{\frac{a^2 + t^2}{b^2 - t^2}},$$

$$S = \sqrt{A^2 - B^2}\sum_{j=1}^{2}\int_{\nu_j}^{b} dt \sqrt{\frac{a^2 + t^2}{b^2 - t^2}}, \quad \text{(A9)}$$

where $\nu_j = \sin\eta_j$, $a^2 = B^2/(A^2 - B^2)$, and $b^2 = 1 - C^2/A^2$. It is possible to write S, C, and their derivatives in terms of elliptic integrals, and it is possible to write down explicit expressions characterizing the error in estimating the geodesic length from (A9), but these formulas are omitted for brevity. Values obtained from (A9) were found to favorably coincide with the centimeter accuracy expected of the computationally quick method provided in Sodano (1965, appendix A).

REFERENCES

Anton, H., 1984: *Elementary Linear Algebra.* John Wiley and Sons, 449 pp.

Boccippio, D. J., and Coauthors, 2000: The Optical Transient Detector (OTD): Instrument characteristics and cross sensor validation. *J. Atmos. Oceanic Technol.,* **17,** 441–458.

Christian, H. J., R. J. Blakeslee, and S. J. Goodman, 1992: Lightning Imaging Sensor (LIS) for Earth Observing System. NASA TM-4350, 36 pp.

Cummins, K. L., E. A. Bardo, W. L. Hiscox, R. B. Pyle, and A. E. Pifer, 1995: A combined TOA/MDF technology upgrade of the U.S. National Lightning Detection Network. Preprints, *Int. Aerospace & Ground Conf. on Lightning and Static Electricity,* Williamsburg, VA, National Interagency Coordination Group, 72-1–72-5.

——, M. J. Murphy, E. A. Bardo, W. L. Hiscox, R. B. Pyle, and A. E. Pifer, 1998: A combined TOA/MDF technology upgrade of the U.S. National Lightning Detection Network. *J. Geophys. Res.,* **103,** 9035–9044.

——, R. B. Pyle, and G. Fournier, 1999: An integrated North American lightning detection network. *Proc. 11th Int. Conf. on Atmospheric Electricity,* Guntersville, AL, NASA Marshall Space Flight Center, 218–221.

Keenan, T., and Coauthors, 1994: Science plan Maritime Continent Thunderstorm Experiment (MCTEX). BMRC Research Rep. 44, 66 pp. [Available from Bureau of Meteorology Research Centre, BMRC, GPO Box 1289K, Melbourne, Victoria 3001, Australia.]

——, R. Carbone, S. Rutledge, J. Wilson, G. Holland, and P. May, 1996: The Maritime Continent Thunderstorm Experiment (MCTEX): Overview and initial results. Preprints, *Seventh Conf. on Mesoscale Processes,* Reading, United Kingdom, Amer. Meteor. Soc., 326–328.

Koshak, W. J., R. J. Blakeslee, and J. C. Bailey, 2000: Data retrieval algorithms for validating the Optical Transient Detector and the Lightning Imaging Sensor. *J. Atmos. Oceanic Technol.,* **17,** 279–297.

Lewis, E. A., 1964: Geometry and first-order error statistics for three- and four-station hyperbolic fixes on a spherical Earth. Upper Atmosphere Physics Laboratory Project 4662, Rep. 29, 88 pp. [Available from Air Force Cambridge Research Laboratories, Office of Aerospace Research, United States Air Force, L. G. Hanscom Field, MA 01731.]

——, R. B. Harvey, and J. E. Rasmussen, 1960: Hyperbolic direction finding with sferics of transatlantic origin. *J. Geophys. Res.,* **65,** 1879–1905.

Orville, R. E., Jr., 1987: An analytic solution to obtain the optimum source location using multiple direction finders on a spherical surface. *J. Geophys. Res.,* **92,** 10 877–10 886.

Sodano, E. M., 1965: General non-iterative solution of the inverse and direct geodetic problems. *Bull. Geodesique (J. Int. Assoc. Geodesy),* **75,** 69–89.

Twomey, S. A., 1977: *Introduction to the Mathematics of Inversion in Remote Sensing and Indirect Measurements.* Elsevier, 243 pp.